J Mater Sci: Mater Electron (2021) 32:18138–18144

Impact of composite last quantum barrier on the performance of AlGaN-based deep ultraviolet light-emitting diode

Liang Lu[1], Xiong Zhang[1,*], Shuchang Wang[2], Aijie Fan[1], Shuai Chen[1], Cheng Li[1], Abbas Nasir[1], Zhe Zhuang[1], Guohua Hu[1], and Yiping Cui[1]

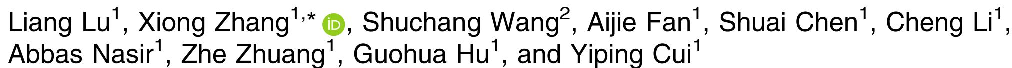

[1] *Advanced Photonics Center, Southeast University, Nanjing 210096, Jiangsu, China*
[2] *College of Electronic and Information Engineering, Changshu Institute of Technology, Changshu 215500, Jiangsu, China*

Received: 6 April 2021
Accepted: 7 June 2021
Published online: 15 June 2021

© The Author(s), under exclusive licence to Springer Science+Business Media, LLC, part of Springer Nature 2021

ABSTRACT

The AlGaN-based deep ultraviolet light-emitting diodes (DUV-LEDs) with a newly developed composite last quantum barrier (CLQB) were studied extensively. The CLQB was composed of a conventional undoped last quantum barrier (u-LQB) and an extra Mg-doped last quantum barrier (p-LQB). It was demonstrated that the light output power of the DUV-LED could be improved significantly by inserting the p-LQB to form the CLQB with carefully optimized Mg-doping level. In fact, the light output power of the AlGaN-based DUV-LED with the optimized CLQB increased by approximately 30% as compared with the DUV-LEDs fabricated without the insertion of the p-LQB at an injection current of 40 mA. Furthermore, it was revealed that the increase in light output power could be ascribed to the introduction of the CLQB, which attenuated the electrical current leakage and increased the hole injection efficiency.

1 Introduction

AlGaN-based III-nitrides with a wide direct energy bandgap tunable from 3.45 (GaN) to 6.28 eV (AlN) exhibit excellent performance in both electronic and optoelectronic devices such as high-frequency high electron mobility transistors (HEMTs) [1, 2], high-sensitivity detectors, and deep ultraviolet light-emitting diodes (DUV-LEDs). In particular, AlGaN-based DUV-LEDs have a wide range of potential applications, such as UV sterilization, medical diagnostics, and water/air purification [3–5]. Up to now, AlGaN-based III-nitrides grown along the polar *c* [0001] direction have been widely used in the research and fabrication of DUV-LEDs. Because the polar AlGaN-based epi-layers with high crystalline quality are easier to obtain than their counterparts with other orientations. The internal quantum efficiency (IQE) of these devices can be severely affected by the quantum-confined Stark effect (QCSE) due to the existence of the spontaneous polarization and the lattice-mismatch-induced piezoelectric polarization [6, 7]. However, the external quantum efficiency (EQE) of DUV-LED grown along the polar *c* [0001] direction is

Address correspondence to E-mail: xzhang62@aliyun.com

https://doi.org/10.1007/s10854-021-06357-9

still approximately an order of magnitude higher than the DUV-LEDs with other orientations. However, the light output power of the DUV-LEDs is still limited by the poor IQE, low carrier injection efficiency, and lousy EQE [8–11]. In particular, it remains a challenge to confine the electrons effectively, while injecting sufficient holes into the active region of the DUV-LED for enhancing the IQE.

So far a variety of innovative methods have been developed to improve IQE, including (1) reducing defects and dislocations in the epitaxial layers [12, 13]; (2) increasing the doping efficiency of n-type and p-type materials to form conductive films for improving current injection efficiency [14, 15]; and (3) the use of novel AlGaN-based quantum well and barrier structure in the active region [16–18]. In addition, researchers have performed various kinds of energy band engineering works to improve IQE, prevent current leakage, and reduce light output power drop during high current injection process. Liu et al. reported a great enhancement in light extraction efficiency for DUV-LED by using a novel AlGaN-delta-GaN QW structure instead of a conventional AlGaN QW structure based on their simulation results [19]. Ren et al. summarized the recent progress in energy band engineering of the DUV-LEDs, with particular attention paid to the band engineering of electron blocking layers, quantum wells, and quantum barriers, and to the implementation of many novel structures such as tunnel junctions and ultra-thin quantum heterostructures utilized to enhance the efficiency [20]. Hao et al. reported the improvement in the current injection efficiency via controlling the relaxation of strains in the p-AlGaN hole injection layer (HIL) and the electron blocking layer (EBL) [21]. Liu et al. reported the use of a composition-graded AlGaN layer as the LQB, replacing the conventional flat LQB to reduce the effective barrier height for improving the hole injection and electron blocking ability [22]. Zhang et al. modified the conventional p-type electron blocking layer (p-EBL) structure by adding a very thin ($\sim$ 3 nm) AlGaN layer [18] or superlattice (SL) [23] or multiple quantum barrier (MQB) structure [23] to improve the hole transport capability. Shih et al. designed an EBL featured with a graded-composition and multi-quantum barrier structure to promote the capabilities of both electron confinement and hole injection, and the light output power [24]. He et al. used an $Al_xGa_{1-x}N$ carrier reservoir layer instead of the conventional single undoped last quantum barrier to enhance the IQE and alleviate the efficiency droop phenomenon [25]. In spite of these efforts, the IQE of AlGaN-based DUV-LEDs is still far below that of the GaN-based blue LEDs. Therefore, the IQE of AlGaN-based DUV-LEDs needs to be further enhanced to replace the toxic mercury lamps as the UV light sources for practical applications.

In this study, the impact of the newly developed Mg-doped composite last quantum barrier (CLQB) comprising a conventional undoped last quantum barrier layer (u-LQB) and an extra Mg-doped last quantum barrier layer (p-LQB) on the light output power and other characteristics of the AlGaN-based DUV-LEDs was investigated intensively. The characterization results reveal that a significant increase in light output power of the AlGaN-based DUV-LEDs could be achieved by employing the CLQB with optimized Mg-doping level.

2 Experimental

All the AlGaN-based DUV-LED samples used in this study were grown on 2-inch (0001) c-plane sapphire substrates in a vertical low-pressure cold-wall metal organic chemical vapor deposition (MOCVD) system. Ammonia (NH_3), silane (SiH_4), trimethyl-aluminum (TMAl), trimethyl-gallium (TMGa), and bicyclopentadienyl-magnesium (Cp_2Mg) were used as the precursors for N, Si, Al, Ga, and Mg, respectively. Hydrogen (H_2) was used as the carrier gas. At the beginning of the MOCVD growth process, the c-plane sapphire substrate was heated up to 1060 °C to remove the surface contamination for all the samples in H_2 atmosphere. Then, the temperature was lowered down to 750 °C to grow a low-temperature (LT) AlN nucleation layer. After that, a 2.5-μm-thick AlN buffer layer was grown in three steps. At the first step, the growth of the AlN buffer layer was initiated at a temperature of 1250 °C with a V/III ratio of 570. The growth of the AlN epi-layer proceeded and did not start the second step until the layer thickness reached a value of 750 nm. Then, the V/III ratio was decreased to 285 and the temperature was decreased to 1220 °C to continue growing 1.2 μm thick more AlN film. Subsequently at the third step, the last 550 nm-thick AlN buffer layer was grown with the V/III ratio identical to that used at the second step and the temperature set to 1200 °C. The rest

layer structure of the AlGaN-based DUV-LED was composed of a 30-period undoped $AlN/Al_{0.55}Ga_{0.45}N$ superlattice (SL) which was followed by a 2.5-μm-thick n-$Al_{0.68}Ga_{0.32}N$ epi-layer and 6 pairs of multiple quantum wells (MQWs) comprising 1.6-nm-thick $Al_{0.34}Ga_{0.66}N$ wells and 12-nm-thick $Al_{0.59}Ga_{0.41}N$ barriers. After that, the composite last quantum barrier (CLQB) comprising a 14-nm-thick undoped $Al_{0.59}Ga_{0.41}N$ last quantum barrier (u-LQB) and an extra 6-nm-thick p-$Al_{0.59}Ga_{0.41}$ N last quantum barrier with Mg-doped at various levels (p-LQB) was grown over the MQWs. Next, 4 periods of Mg-doped p-$Al_{0.6}Ga_{0.4}N/Al_{0.4}Ga_{0.6}N$ SL EBL were grown on the CLQB. Finally, an Al composition-graded Mg-doped p-AlGaN layer and a Mg-doped p-GaN contact layer were grown on the EBL. The schematic layer structure of the AlGaN-based DUV-LEDs is shown in Fig. 1. Six samples named as samples A-F were grown in this study. Sample A was used as the reference sample which had only 14-nm-thick LQB. The 6-nm-thick Mg-doped p-$Al_{0.59}Ga_{0.41}$ N last quantum barrier (p-LQB) was inserted in between the undoped 14-nm-thick $Al_{0.59}Ga_{0.41}N$ (u-LQB) and the Mg-doped SL EBL for samples B-F. And samples B-F were grown with the Cp_2Mg flow rate of 0.03, 0.05, 0.08, 0.12, and 0.16 μmol/min, respectively. The activation of Mg-doped epi-layers for all the AlGaN-based DUV-LED samples was executed with the thermal annealing technique at 700 °C for 15 min in nitrogen ambient. The six AlGaN-based DUV-LED samples A-F were characterized at room temperature (RT) by using electroluminescence (EL) and photoluminescence (PL) spectra in addition to electrical current–voltage (I–V) measurement. The excitation wavelength for the PL measurement was 244 nm, and both the PL and EL spectra were measured from the p-contact side of the LED wafer.

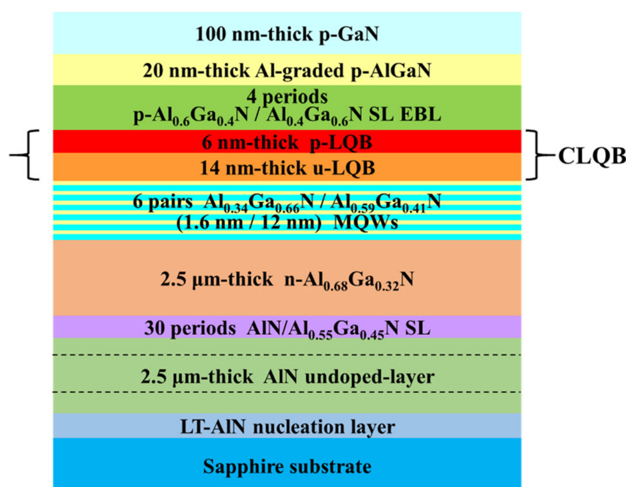

Fig. 1 The schematic layer structure for the AlGaN-based DUV-LED samples B–F grown with the insertion of Mg-doped p-LQB. The reference sample (sample A) has nearly the same layer structure as samples B–F except for the lack of the p-LQB layer

3 Results and discussion

The EL spectra for the six DUV-LED samples measured at RT are shown in Fig. 2. The inserted figure demonstrates the enlarged EL spectra near 310 nm. Besides the major emission peak near 275 nm, an unambiguous parasitic emission peak located at approximately 310 nm can be observed for all the samples except for sample A. And it is evident that the EL intensities of these parasitic emissions are strongly dependent on the Mg-doping level. In fact, the more Mg is incorporated, the larger the parasitic emission peak intensity is. However, until now there are quite a lot explanations or speculations for the physical origin of this parasitic emission. Zhang et al. believed that the parasitic emission was related to the injected electrons into the p-AlGaN layer of the device structure [26]. Shatalov et al. pointed out that the long-wavelength emission band centered at 330 nm was caused by the carrier recombination from the conduction band to the deep acceptor levels in the energy bandgap of the p-AlGaN layer at RT [27].

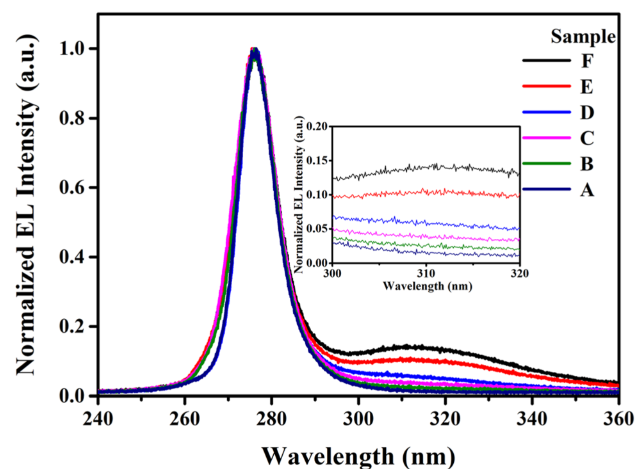

Fig. 2 The normalized RT EL spectra of sample A and samples B-F with p-LQB doped with the Cp_2Mg flow rate of 0.03, 0.05, 0.08, 0.12, and 0.16 μmol/min, respectively

As shown in Fig. 2, the sub-band parasitic emission was not observed in the EL spectrum of sample A grown without the CLQB, whereas the sub-band parasitic emission was remarkable in the EL spectra for all the other samples with the CLQB including sample B which was just slightly doped with Mg. And the I–V data for sample B grown with the p-LQB doped at a Cp_2Mg flow rate of 0.03 μmol/min are shown in Fig. 3. The overflow of electrons from the quantum wells of the active region into the p-LQB layer and the subsequent recombination of electrons and holes in the p-LQB layer are considered in this study to be responsible for this parasitic emission. Similar phenomenon was also observed in the PL spectra shown in Fig. 4 although the PL intensity ratio of the parasitic emission vs. the major emission was generally smaller than that in the EL spectra. The inserted figure is the enlarged PL spectra near 310 nm. The EL and PL intensity ratios of the parasitic emission peak vs. the major emission peak for samples A-F are summarized in Table 1. This result can be explained in terms of the less number of the excited electrons in the quantum well structure and thus less overflow of electrons into the p-LQB layer in the measurement process of PL spectrum than that of the excited electrons in the measurement process of the EL spectrum.

The energy bandgap of $Al_xGa_{1-x}N$ alloy can be written as a function of Al composition x:

$$E_g(x) = xE_g(\mathrm{AlN}) + (1-x)E_g(\mathrm{GaN}) - bx(1-x), \quad (1)$$

where the bowing parameter b is 1 eV, and the energy bandgaps of GaN and AlN are 3.45 eV and

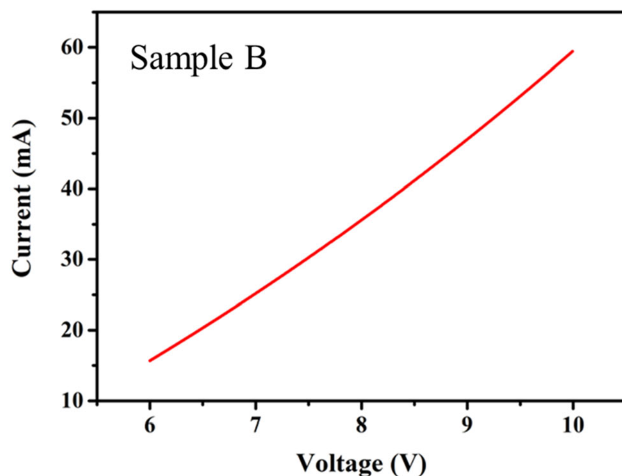

Fig. 3 The I–V characteristic of sample B grown with the p-LQB doped at a Cp_2Mg flow rate of 0.03 μmol/min

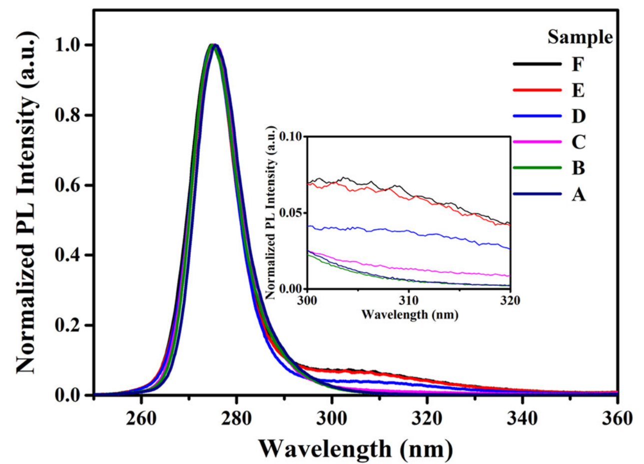

Fig. 4 The normalized RT PL spectra of samples A and samples B–F with p-LQB doped with the Cp_2Mg flow rate of 0.03, 0.05, 0.08, 0.12, and 0.16 μmol/min, respectively

Table 1 The EL and PL intensity ratios of the parasitic emission peak vs. the major emission peak for samples A–F

Sample	A	B	C	D	E	F
R_{EL}	0.000	0.025	0.036	0.063	0.107	0.146
R_{PL}	0.000	0.007	0.013	0.038	0.063	0.068

6.28 eV, respectively. The band offset of the AlGaN alloy with respect to GaN was taken as 70% for conduction band and 30% for valence band [28]. The relationship between the Mg acceptor energy level $E_A(x)$, the impurity-related emission energy $E_{emi}(x)$, and the nitrogen-vacancy-related energy level of V_N^{1+} in $Al_xGa_{1-x}N$ alloy as a function of x can be expressed as

$$E_{V_N^{1+}}(x) = E_g(x) - E_{emi}(x) - E_A(x). \quad (2)$$

In this study, the Al composition of p-LQB x was determined to be approximately 59%, i.e., $x = 0.59$. According to formula (1), $E_g(x)$ can be calculated to be 4.88 eV. The energy level of i_N^{1+} was known to be 0.26 eV in AlN [29]. $E_A(x) = E_{GaN}(Mg^0) + E_V$, where the energy level of neutral Mg $E_{GaN}(Mg^0)$ is 0.17 eV in GaN [30] and $E_V = -0.3\Delta E_g(x) = 0.43$ eV. Therefore, $E_A(x) = 0.17 + 0.43 = 0.6$ eV, and E_{emi} can be calculated to be 4.02 eV based on formula (2), corresponding to a wavelength of 308 nm which is very close to the observed impurity-related emission wavelength 310 nm. Therefore, the sub-band parasitic emission peak should be originated from the

impurity-related transition. The energy band structure and the energy levels associated with V_N^{1+} donor and Mg^0 acceptor together with the optical transition between $E_{V_N^{1+}}$ and E_{Mg^0} in GaN and Mg-doped $Al_{0.59}Ga_{0.41}N$ p-LQB are shown in Fig. 5a. [31] And the schematic diagram of the energy band lineup near the p-CLQB is shown in Fig. 5b.

On the other hand, the relationship between the light output power and the injection current (L–I) under the application of DC power is shown in Fig. 6a. To facilitate the comparative analysis of the experimental results, the light output power of sample B obtained at 60 mA is taken as the basis, and the light output power of other samples is normalized based on this power. It can be seen clearly from Fig. 6a that the difference in light output power between samples A-F is quite small at low injection currents. However, when the injection current is above 30 mA, the impact of the introduction of the CLQB on the light output power of the AlGaN-based DUV-LED becomes apparent. In particular, as shown in Fig. 6b, under an injection current of 40 mA, a steep 30% increase in light output power of the device was achieved when the Cp_2Mg flow rate was increased from 0 for sample A to 0.03 μmol/min for sample B with slightly Mg-doped p-LQB. However, the light output power decreases monotonously as the Cp_2Mg flow rate was further increased. In fact, when the Cp_2Mg flow rate was increased to 0.08 μmol/min for sample D, the light output power of sample D was almost the same as that of sample A grown without the insertion of the p-LQB layer. The variation trend for the light output power as a function of the Mg-doping level in the p-LQB can be explained as follows. On the one hand. the introduction of the CLQB with Mg properly doped in the p-LQB layer can help to block the overflowing electrons and attenuate the electrical current leakage due to electron overflow. On the other hand, the p-LQB can enhance the hole injection efficiency by generating more holes inside the MQWs, resulting in more effective radiative recombination and thus higher light output power than that of the DUV-LED grown without the CLQB [32–34]. However, as the Cp_2Mg flow rate or Mg-doping level was further increased (samples C-F), the light output power can decrease significantly because the excessive Mg-doping in the p-LQB layer can induce the surge in the impurity-related sub-band parasitic emissions. Therefore, for suppressing the sub-band parasitic emissions, the Mg-doping level for the inserted p-LQB has to be optimized to achieve the highest light output power for the AlGaN-based DUV-LEDs.

4 Conclusions

The AlGaN-based DUV-LEDs with a novel CLQB comprising a conventional undoped last quantum barrier (u-LQB) and an extra Mg-doped last quantum barrier (p-LQB) were successfully fabricated. It was demonstrated that the light output power of the AlGaN-based DUV-LEDs could be enhanced significantly by inserting the p-LQB layer to form the CLQB with carefully optimized Mg-doping level. In fact, an approximately 30% increase in light output power was achieved with the AlGaN-based DUV-LED

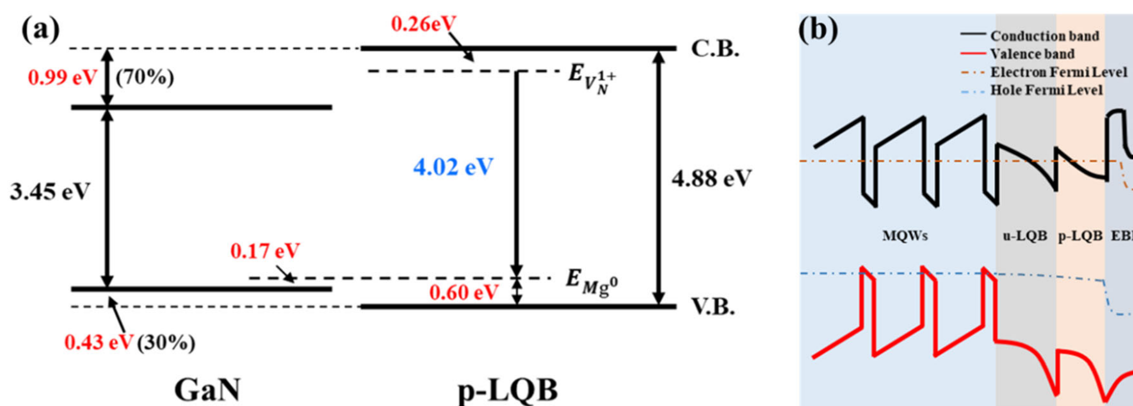

Fig. 5 The energy band structure and the energy levels associated with V_N^{1+} donor and Mg^0 acceptor together with the optical transition between $E_{V_N^{1+}}$ and E_{Mg^0} in GaN and Mg-doped $Al_{0.59}Ga_{0.41}$ N p-LQB (**a**); the schematic diagram of the energy band lineup near the p-CLQB (**b**)

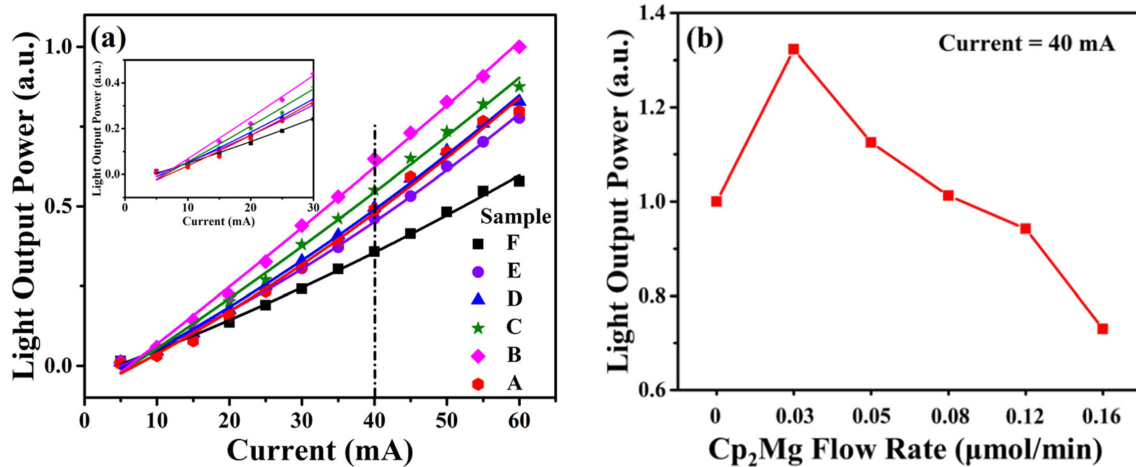

Fig. 6 The L–I characteristics of samples A–F (**a**); the relative light output power as a function of the Cp_2Mg flow rate with respect to the light output power of sample A under an injection current of 40 mA (**b**)

grown with the optimized CLQB as compared with the DUV-LED fabricated without the insertion of the p-LQB or the DUV-LEDs with excessive Mg doped in the p-LQB layer. Moreover, it was revealed that the increase in light output power could be ascribed to the blocking effect of the CLQB to the overflowing electrons, which attenuated the electrical current leakage and increased the hole injection efficiency.

Acknowledgements

This work was supported by the National Natural Science Foundation of China (Grant No. 62005026), Natural Science Foundation of Jiangsu Province (Grant No. BK20191027), National Natural Science Foundation of China (Grant No. 61804027), and Natural Science Foundation of Jiangsu Province (Grant No. BK20180359).

References

1. T. Aggerstam, S. Lourdudoss, H.H. Radamson, M. Sjödin, P. Lorenzini, D.C. Look, Thin Solid Films **515**, 705–707 (2006)
2. T. Nanjo, A. Imai, Y. Suzuki, Y. Abe, T. Oishi, M. Suita, E. Yagyu, Y. Tokuda, IEEE Trans. Electron Devices **60**, 1046–1053 (2013)
3. A. Khan, K. Balakrishnan, T. Katona, Nat. Photonics **2**, 77–84 (2008)
4. W. Sun, M. Shatalov, J. Deng, X. Hu, J. Yang, A. Lunev, Y. Bilenko, M. Shur, R. Gaska, Appl. Phys. Lett. **96**, 061102 (2010)
5. M.S. Shur, R. Gaska, IEEE Trans. Electron Devices **57**, 12–25 (2010)
6. H. Masui, S. Nakamura, S.P. DenBaars, U.K. Mishra, IEEE Trans. Electron Devices **57**, 88–100 (2010)
7. T. Paskova, Physica Status Solidi (B) **245**(6), 1011–1025 (2008)
8. W. Guo, H. Sun, B. Torre, J. Li, M. Sheikhi, J. Jiang, H. Li, S. Guo, K.-H. Li, R. Lin, A. Giugni, E. Di Fabrizio, X. Li, J. Ye, Adv. Funct. Mater. **28**, 1802395 (2018)
9. H. Sun, M.K. Shakfa, M.M. Muhammed, B. Janjua, K.-H. Li, R. Lin, T.K. Ng, I.S. Roqan, B.S. Ooi, X. Li, ACS Photonics **5**, 964–970 (2017)
10. H. Sun, D. Priante, J.-W. Min, R.C. Subedi, M.K. Shakfa, Z. Ren, K.-H. Li, R. Lin, C. Zhao, T.K. Ng, J.-H. Ryou, X. Zhang, B.S. Ooi, X. Li, ACS Photonics **5**, 3305–3314 (2018)
11. Z. Zhuang, D. Iida, K. Ohkawa, Opt. Express **28**, 30423 (2020)
12. H. Long, J. Dai, Y. Zhang, S. Wang, B. Tan, S. Zhang, L. Xu, M. Shan, Z.C. Feng, C. Chen, H.. Kuo, Appl. Phys. Lett. **114**, 042101 (2019)
13. Z. Chen, J. Hoo, Y. Chen, V. Wang, S. Guo, Jpn. J. Appl. Phys. **58**, SC1007 (2019)
14. Y. Li, C. Wang, Y. Zhang, P. Hu, S. Zhang, M. Du, X. Su, Q. Li, F. Yun, Photonics Res. **8**, 806 (2020)
15. Q. Chen, J. Dai, X. Li, Y. Gao, H. Long, Z.-H. Zhang, C. Chen, H.-C. Kuo, IEEE Electron Device Lett. **40**, 1925–1928 (2019)
16. H. Hu, B. Tang, H. Wan, H. Sun, S. Zhou, J. Dai, C. Chen, S. Liu, L.J. Guo, Nano Energy **69**, 104427 (2020)
17. H. Sun, S. Mitra, R.C. Subedi, Y. Zhang, W. Guo, J. Ye, M.K. Shakfa, T.K. Ng, B.S. Ooi, I.S. Roqan, Z. Zhang, J. Dai, C. Chen, S. Long, Adv. Funct. Mater. **29**, 1905445 (2019)

18. Z.H. Zhang, S.W.H. Chen, Y.H. Zhang, L.P. Li, S.W. Wang, K.K. Tian, C.S. Chu, M.Q. Fang, H.C. Kuo, W.G. Bi, ACS Photonics **4**, 1846–1850 (2017)
19. C. Liu, B. Melanson, J. Zhang, Photonics Res. **7**, 87 (2020)
20. Z. Ren, H. Yu, Z. Liu, D. Wang, C. Xing, H. Zhang, C. Huang, S. Long, H. Sun, J. Phys. D Appl. Phys. **53**, 073002 (2020)
21. G.-D. Hao, M. Taniguchi, S.-I. Inoue, J. Phys. D Appl. Phys. **53**, 505107 (2020)
22. Z. Liu, H. Yu, Z. Ren, J. Dai, C. Chen, H. Sun, Semicond. Sci. Technol. **35**, 075021 (2020)
23. Z.H. Zhang, S.W. Huang Chen, C. Chu, K. Tian, M. Fang, Y. Zhang, W. Bi, H.C. Kuo, Nanoscale Res. Lett. **13**, 122 (2018)
24. Y.-H. Shih, J.-Y. Chang, J.-K. Sheu, Y.-K. Kuo, F.-M. Chen, M.-L. Lee, W.-C. Lai, IEEE Trans. Electron Devices **63**, 1141–1147 (2016)
25. L. He, W. Zhao, K. Zhang, C. He, H. Wu, X. Liu, X. Luo, S. Li, Z. Chen, Appl. Phys. Express **12**, 062013 (2019)
26. J. Zhang, S. Wu, S. Rai, V. Mandavilli, V. Adivarahan, A. Chitnis, M. Shatalov, M.A. Khan, Appl. Phys. Lett. **83**, 3456–3458 (2003)
27. M. Shatalov, A. Chitnis, V. Mandavilli, R. Pachipulusu, J.P. Zhang, V. Adivarahan, S. Wu, G. Simin, M.A. Khan, G. Tamulaitis, A. Sereika, I. Yilmaz, M.S. Shur, R. Gaska, Appl. Phys. Lett. **82**, 167–169 (2003)
28. M.L. Nakarmi, N. Nepal, J.Y. Lin, H.X. Jiang, Appl. Phys. Lett. **94**, 091903 (2009)
29. N. Nepal, K.B. Nam, M.L. Nakarmi, J.Y. Lin, H.X. Jiang, J.M. Zavada, R.G. Wilson, Appl. Phys. Lett. **84**, 1090–1092 (2004)
30. K.B. Nam, M.L. Nakarmi, J. Li, J.Y. Lin, H.X. Jiang, Appl. Phys. Lett. **83**, 878–880 (2003)
31. C.-L. Tsai, H.-H. Liu, J.-W. Chen, C.-P. Lu, K. Ikenaga, T. Tabuchi, K. Matsumoto, Y.-K. Fu, Solid-State Electron. **138**, 84–88 (2017)
32. Y.-K. Kuo, M.-C. Tsai, S.-H. Yen, T.-C. Hsu, Y.-J. Shen, IEEE J. Quantum Electron. **46**, 1214–1220 (2010)
33. Z. Jun, T. Wu, W. Feng, Y. Weiyi, X. Hui, D. Jiangnan, F. Yanyan, W. Zhihao, C. Changqing, IEEE Photonics J. **5**, 1600310–1600310 (2013)
34. X. Zhang, H. Sun, J. Huang, T. Liu, X. Wang, Y. Zhang, S. Li, S. Zhang, Y. Hou, Z. Guo, J. Electron. Mater. **48**, 460–466 (2018)

Publisher's Note Springer Nature remains neutral with regard to jurisdictional claims in published maps and institutional affiliations.